ADVANCED FUNCTIONAL MATERIALS
www.afm-journal.de

Ionic Modulation of Interfacial Magnetism in Light Metal/Ferromagnetic Insulator Layered Nanostructures

Mengmeng Guan, Lei Wang, Shishun Zhao, Bin Peng, Wei Su, Zhexi He, Guohua Dong, Tai Min, Jing Ma, Zhongqiang Hu, Wei Ren, Zuo-Guang Ye, Ce-Wen Nan, Ziyao Zhou,* and Ming Liu**

Ferromagnetic insulator thin film nanostructures are becoming the key component of the state-of-the-art spintronic devices, for instance, yttrium iron garnet (YIG) with low damping, high Curie temperature, and high resistivity is explored into many spin–orbit interactions related spintronic devices. Voltage modulation of YIG, with great practical/theoretical significance, thus can be widely applied in various YIG-based spintronics effects. Nevertheless, to manipulate ferromagnetism of YIG through electric field (E-field), instead of current, in an energy efficient manner is essentially challenging. Here, a YIG/Cu/Pt layered nanostructure with a weak spin–orbit coupling interaction is fabricated, and then the interfacial magnetism of the Cu and YIG is modified via ionic liquid gating method significantly. A record-high E-field-induced ferromagnetic resonance field shift of 1400 Oe is achieved in YIG (17 nm)/Cu (5 nm)/Pt (3 nm)/ionic liquid/Au capacitor layered nanostructures with a small voltage bias of 4.5 V. The giant magnetoelectric tunability comes from voltage-induced extra ferromagnetic ordering in Cu layer, confirmed by the first-principle calculation. This E-field modulation of interfacial magnetism between light metal and magnetic isolator may open a door toward compact, high-performance, and energy-efficient spintronic devices.

1. Introduction

The interface between heavy metal and ferromagnetic insulator (FMI) heterojunctions serves as important building block in spintronics for its capability of interconversion between spin and current. yttrium iron garnet (YIG), which has low magnetic damping constant ($\alpha \approx 10^{-5}$), high Curie temperature ($T_C \approx 650$ K), and very narrow ferromagnetic resonance (FMR) linewidth (≈1 Oe), is an ideal FMI. It has been demonstrated that YIG exhibits a plenty of spintronic couplings with the heavy metals like Pt, Ta, and W. These spintronic behaviors like spin pumping,[1] spin Hall,[2] spin Seebeck,[1,3] and magnetic proximity effect (MPE)[4,5] in YIG/heavy metal layered nanostructures have attracted increasing research interests these years.[1,3,6–11] Current-driven spin–orbit torque (SOT),[12] where in particular, the SOT in the YIG/heavy metal interface,[13] is a hot topic in these researches. Consequently, the task of tuning of ferromagnetism is converted into to procure the high conversion efficiency between spin and charge currents, where the heavy metals with strong spin–orbit interaction (SOI) play as key component.

Nevertheless, the state-of-the-art maximal of 10% conversion efficiency in noble metal Pt is still limited.[14] Additionally, seeking heavy metal layer for spin and charge current conversion limits the selection of materials, and raises the cost of real spintronic applications. Even with much cheaper cost, light metals (LMs) like Cu with weak SOI have been excluded from SHE devices. Surprisingly, Prof. Ando's group revealed that the nature oxidation of Cu layer reaches the comparable conversion efficiency of Pt,[15] opening a creative path of magnetization modulation via LMs. Here, we utilize an alternative approach of ionic liquid gating (ILG) to tune ferromagnetism at light metal/FMI interfaces, where ILG generates large charge accumulation at the surfaces and influence the magnetism as an interfacial nanoeffect. It is highly expected that the ionic doping will transform the Cu condition and change the interfacial magnetization accordingly. Moreover, ILG method has much lower energy consumption, than that of spin or charge currents, due to negligible current flow.[16–21]

In this work, we first epitaxially deposited YIG thin films with thickness at 7 and 17 nm onto gadolinium gallium garnet

M. Guan, S. Zhao, Dr. B. Peng, W. Su, Z. He, G. Dong, Prof. Z. Hu, Prof. W. Ren, Prof. Z.-G. Ye, Prof. Z. Zhou, Prof. M. Liu
Electronic Materials Research Laboratory, Key Laboratory of the Ministry of Education & International Center for Dielectric Research
School of Electronic and Information Engineering
State Key Laboratory for Mechanical Behavior of Materials
Xi'an Jiaotong University
Xi'an 710049, China
E-mail: pengbin@xjtu.edu.cn; ziyaozhou@xjtu.edu.cn; mingliu@xjtu.edu.cn

Dr. L. Wang, Prof. T. Min
Center for Spintronics and Quantum System
State Key Laboratory for Mechanical Behavior of Materials
School of Materials Science and Engineering
Xi'an Jiaotong University
Xi'an, Shaanxi 710049, China

Prof. J. Ma, Prof. C.-W. Nan
State Key Lab of New Ceramics and Fine Processing
School of Materials Science and Engineering
Tsinghua University
Beijing 100084, China

Prof. Z.-G. Ye
Department of Chemistry and 4D LABS
Simon Fraser University
Burnaby, British Columbia V5A 1S6, Canada

DOI: 10.1002/adfm.201805592

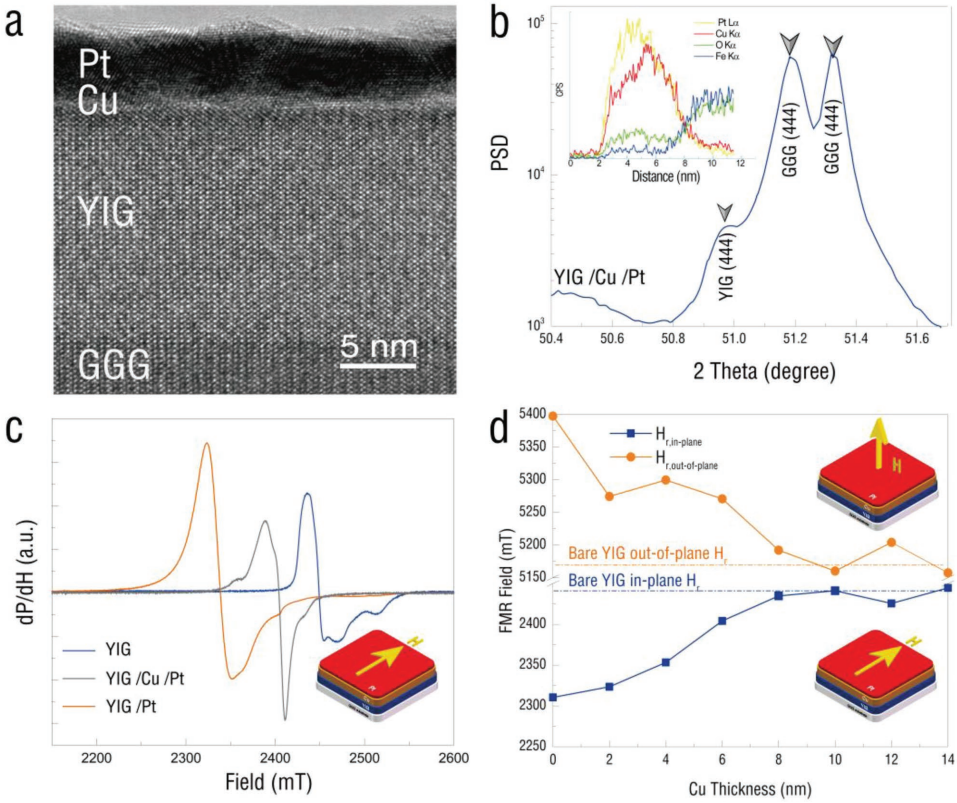

Figure 1. Materials properties and influence of Cu layer on the magnetic properties. a) The cross-section TEM of the GGG/YIG (17 nm)/Cu (5 nm)/Pt (3 nm) sample. b) The XRD pattern of the as-deposited YIG/GGG sample. c) In-plane FMR spectra of the YIG (17 nm) (blue), YIG (17 nm)/Pt (3 nm) (green), and YIG (17 nm)/Cu (5 nm)/Pt (3 nm) (red) samples. d) FMR field dependence on the thickness of the Cu layer between the YIG (17 nm) layer and Pt (3 nm) layer.

($Gd_3Ga_5O_{12}$, GGG) single-crystal substrates using pulsed laser deposition (PLD) system. Then the samples were transferred into a magnetic sputtering chamber, the Cu layer with different thickness (0–14 nm) and 3 nm Pt were then coated onto them subsequently. The Cu layer here served as the coupling media between the YIG and ionic liquid (IL). The Pt served as the protection layer and the gating electrode. By adding an IL layer onto these YIG/Cu/Pt layered nanostructures, we established a typical capacitor structure. When a small gating voltage $V_g = 4.8$ V was applied across the IL layer, a record-high voltage-induced FMR field shift of 1400 Oe was obtained in the YIG (17 nm)/Cu (5 nm)/Pt (3 nm) at −115 °C. The first-principle calculation demonstrated that with the increase of electric field (E-field) across the IL, the positive charge of the interface Cu layer will increase, the nonmagnetic feature remains only about $Cu^{0.6+}$ and then comes up a magnetic state. Thus, the spin ordering of the layered nanostructures will be enhanced and the FMR field will shift accordingly. The magnetic coupling between Cu and YIG is usually negligible weak and the YIG is also a perfect medium in radio frequency and microwave devices such as filters,[22–24] shifter,[25] and isolators.[26] Thereby, we believe that this new ME gating mechanism by inducing a MPE between the YIG and light metal Cu via the unique ILG method is of both fundamental and application potential. The giant FMR tunability in this YIG-based heterostructure will open a door toward the tunable spintronics devices like spin wave transistors or tunable RF/microwave devices such as low-voltage tunable shifters.

The YIG layers are deposited using PLD method with 17 nm thickness. The Cu layers with various thicknesses and 3 nm Pt layers are then deposited on the YIG layer using the magnetic sputtering, details can be seen in the Experimental Section. **Figure 1**a shows the cross-section transmission electron microscopy (TEM) image of the GGG/YIG (17 nm)/Cu (2 nm)/Pt (3 nm) sample. The crystal lattice of the YIG layer indicates a (111) orientation epitaxy growth, the Cu and Pt layer can also be clearly seen on the YIG layer. The X-ray diffraction pattern of the as-deposited 17 nm YIG on GGG substrate is shown in Figure 1b, the (111) peak of the YIG conforms the TEM result. The inset in Figure 1b is the energy-dispersive spectrum of the metal layer, which also shows the layer distribution of Cu and Pt. The in-plane magnetic hysteresis loops of the YIG (17 nm) sample before and after the Pt (3 nm) and Cu (5 nm)/Pt (3 nm) capping are shown in Figure S1 (Supporting Information). After the capping of Pt (3 nm) capping, the hysteresis loop, as shown in blue curve, becomes quadrate in shape. While after the inserting of the Cu (5 nm) layer between the YIG and Pt layer, the magnetic hysteresis loop, as represented in the red curve, exhibits very little difference compared with the hysteresis loop of the bare YIG film. The magnetic hysteresis loops indicating that the ferromagnetic ordering (FM) was enhanced after the Pt (3 nm) capping, and the enhancement can be

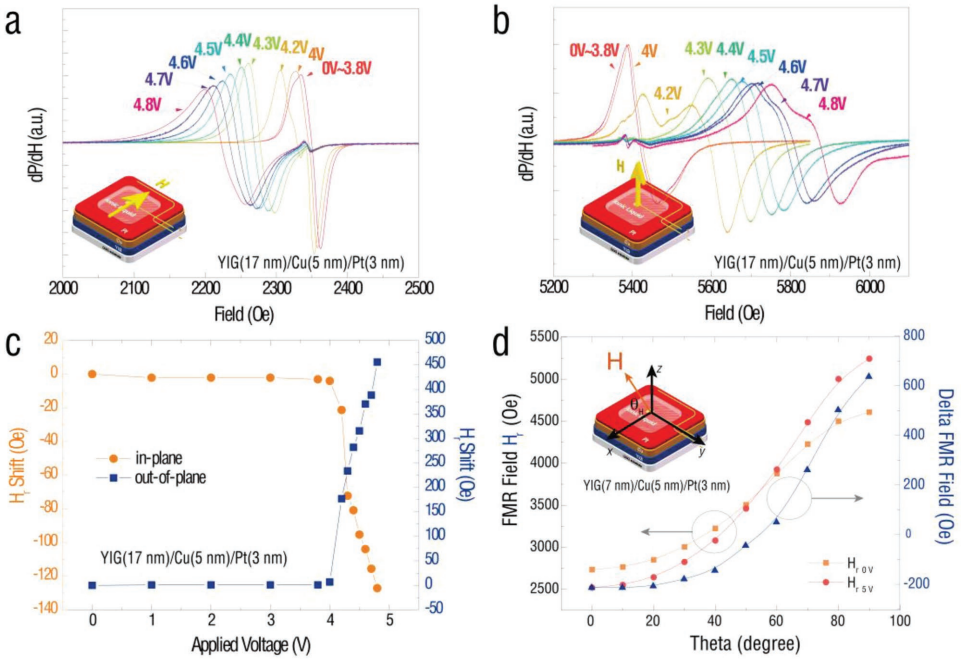

Figure 2. E-field tuning of the magnetic response of the YIG/Cu/Pt samples. a) The in-plane FMR spectra of the YIG (17 nm)/Cu (5 nm)/Pt (3 nm) under sequential gating voltages measured at room temperature. b) The in-plane FMR spectra of the YIG (17 nm)/Cu (5 nm)/Pt (3 nm) under sequential gating voltages measured at room temperature. c) In-plane and out-of-plane FMR field shift dependence on the gating voltage. d) Angular dependence of the FMR field of the YIG (7 nm)/Cu (5 nm)/Pt (3 nm)/IL/Au heterostructure (orange-square line for the initial state and red-round line for the 4.5 V states) and the angular dependence of the ILG-induced FMR shift (blue-triangle line) at room temperature.

eliminated by inserting the Cu (5 nm) layer between the YIG and Pt layer. We also apply FMR spectrometer to monitor the change of magnetic moment of these samples. The FMR effect can be expressed with the Kittel formula

$$f = (\gamma/2\pi)\sqrt{H_r^2 + H_r M_s} \quad (1)$$

for the in-plane condition and

$$f = (\gamma/2\pi)(H_r - M_s) \quad (2)$$

for the out-of-plane condition,[27,28] where f is the frequency of the microwave, $\gamma/2\pi$ = 2.8 (MHz/Oe) is the gyromagnetic ratio,[28] and M_s is the saturation magnetization. In our experiment, all the frequency was set as 9.2 GHz as a limitation of the instrument. As the microwave frequency is fixed in the cavity, the verity of M_s can be quantitatively calculated by the FMR field shift. Figure 1c shows in-plane FMR spectra of the bare YIG (17 nm), YIG (17 nm)/Pt (3 nm), and YIG (17 nm)/Cu (3 nm)/Pt (3 nm). With Pt capping, the in-plane H_r became smaller, implying a strengthened FM ordering, which is consistent with the hysteresis loop change after Pt capping. As expected, the FMR spectra shift in the YIG (17 nm)/Cu (5 nm)/Pt (3 nm) heterostructure decreases compared with that of the YIG/Pt sample. The hysteresis loop changes and the shift in FMR field in YIG after the Pt capping is caused by the magnetic proximity effect (MPE), which has been studied in many articles[4,8,11,29] and is originated from the coupling between Pt 5d and Fe 3d electrons. The decrease in hysteresis loop shape change and FMR shift after the insertion of Cu space layer also indicate the weak coupling between the YIG layer and Cu layer, which is further proved by recording the FMR field shift in YIG/Cu as shown in Figure S3 (Supporting Information), the FMR field was almost the same between YIG (17 nm) and YIG (17 nm)/Cu heterostructure of different Cu thickness. The Cu space layer thickness dependence of both the in-plane and out-of-plane FMR shift is also recorded and shown in Figure 1d. With the increasing of the Cu thickness, the in-plane FMR field increased and out-of-plane FMR field decreased, both saturated at a Cu thickness of 8 nm. The saturation field of the YIG (17 nm)/Cu/Pt (3 nm) was near that of the bare YIG, which also proved the weak coupling between YIG and Cu layer.

As mentioned above, the FM ordering of Pt layers in the proximity of the YIG film results in a torque on the YIG magnetization and manifests it as a shift in the FMR field. Our early study proved that extra magnetic moment of Pt can be induced via the ILG process and thus the MPE would be enhanced with corresponding FMR field shift. However, it seems that the heavy metal Pt is necessary in electric tuning of the magnetic properties of YIG. So here comes an interesting question, what will happen if we apply this ILG method on the YIG/Cu/Pt, where light metal Cu is at the interface?

In situ ILG process on the YIG/Cu/Pt is monitored in the FMR cavity with the schematic of the gating process shown in the inset of **Figure 2**a,b,d. The samples can be rotated with the sample holder to verify the magnetic field direction. The temperature can also be changed in the cavity. Under a positive V_g, the anions ($TSFI^+$) and cations ($DEME^-$) inside IL migrate toward the Cu/Pt electrode and Au electrode, respectively. The anions generate an enormous surface charge density up to 10^{15} cm^{-2},

producing a strong interfacial E-field at the IL/Pt interface. Figure 2a,b shows the in-plane and out-of-plane FMR curves of the YIG (17 nm)/Cu (5 nm)/Pt (3 nm) under different gating voltage, respectively. At room temperature, the FMR field shift increase with the increasing of the gating bias voltage. The in-plane set and out-of-plane field shift show opposite tendency with the increasing of the gating voltage. As can be dedicated from Equations (1) and (2), the FMR shift in our experiment signify a gain of the magnetic moment in the sample. Both the in-plane and out-of-plane FMR field shift dependent on the gating voltage are shown in Figure 2c, a maximum FMR shift of 480 Oe toward the high end is achieved along the out-of-plane direction under 4.8 V gating voltage at room temperature, corresponding to a magnetic-electric (ME) tunability of 100 Oe V^{-1}. Figure 2d shows the angular dependence FMR field of the as-grown YIG (7 nm)/Cu (5 nm)/Pt (3 nm) and 4.8 V gated sample, as well as the ILG-induced FMR shift, respectively. The maximum FMR field shift of this sample is 633 Oe achieved in the out-of-plane direction. The room temperature tunability of this sample is 131 Oe V^{-1}, which is even larger than that of the YIG (17 nm)/Cu (5 nm)/Pt (3 nm) sample. The magnetic coupling is essentially an interfacial effect between YIG and metal. The larger tunability is originated from the smaller thickness of YIG.

The in-plane FMR curve of the YIG (17 nm)/Cu (5 nm)/Pt (3 nm) under temperature from −115 to 25 °C is shown in **Figure 3**a. With the decreasing of temperature, the thermal distribution decreases, thus the effective magnetic moment in the sample increases accordingly, then the FMR field shifts as the result of the increasing magnetic moment. The influence of ambient temperature during the ILG process is also analyzed and shown in Figure 3b,c. The variation between the initial state and 4.5 V gating state of the YIG (17 nm)/Cu (5 nm)/Pt (3 nm) is recorded. Interestingly, with decreasing the temperature, the H_r shift induced by the ILG increased. A much greater FMR shift of 1400 Oe with the out-of-plane magnetic bias is achieved at −115 °C via IL gating in the YIG (17 nm)/Cu (5 nm)/Pt (3 nm) sample. With temperature decreasing, there appeared a stronger magnetic coupling between the YIG and Cu interface, which is evidenced by the larger H_r difference between the in-plane and the out-of-plane direction. This effect can be explained as: the thermal distribution under low temperature is much lower and the ME effect is thereby enhanced relatively. This phenomenon also appears in other multiferroics systems like Ni-doped $LaAlO_3/SrTiO_3$,[30] perpendicular magnetic anisotropy (PMA) structures,[31] etc. As mentioned above, the voltage we applied on the Au electrode was positive and that on the Pt/Cu is negative. We defined this electric field direction as the P state, which can drive the cations to the Pt end. On the contrary, the N state is defined as the negative voltage was applied on the gold wire. The out-of-plane FMR shift of a YIG (17 nm)/Cu (2 nm)/Pt (3 nm) sample under the N state and P state is shown in Figure 3d. Negative voltage is applied gradually to −4.5 V first, the FMR field decreases with increasing the gating voltage. When the voltage is decreased to 0 V, the FMR field increases accordingly. Similarly, in YIG (17 nm)/Cu (5 nm)/Pt (3 nm), the resonance field increase with increasing the gating voltage. Surprisingly, the FMR field decrease with the repeal of the gating voltage. Besides, the reversibility of FMR switching is also studied, as illustrated in Figure S2

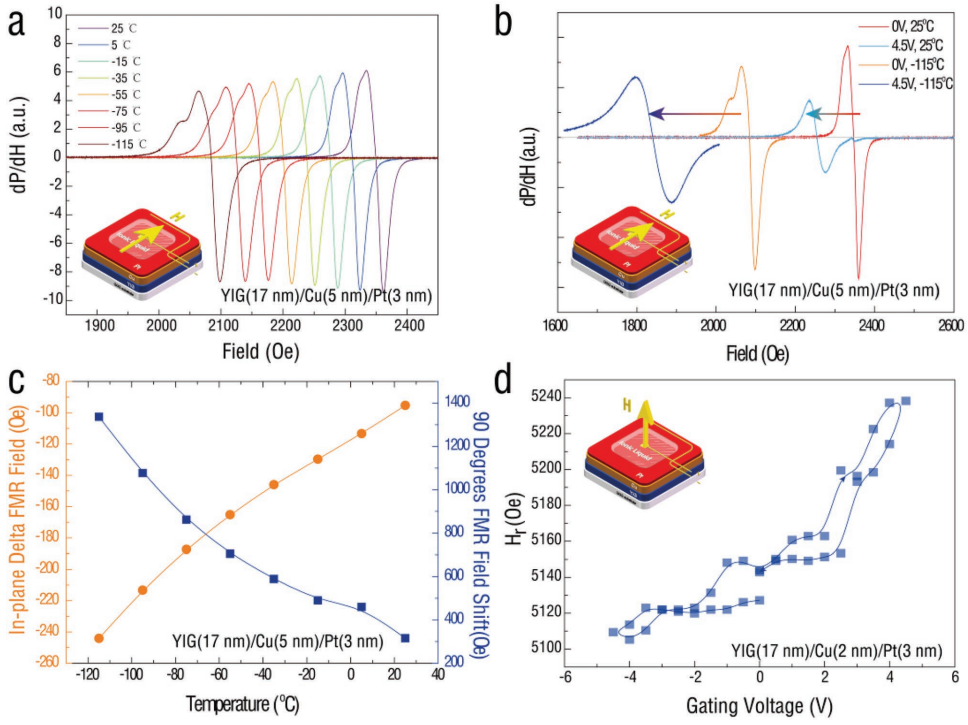

Figure 3. The influence of the gating temperature and reversible gating voltage on the gating process. a) The FMR shift on the YIG (17 nm)/Cu (2 nm)/Pt (3 nm) under different voltage from −4.5 to 4.5 V ILG voltage alone the out-of-plane at room temperature. b) The reproducible test of the gating process in YIG (17 nm)/Cu (2 nm)/Pt (3 nm) along the out-of-plane at room temperature.

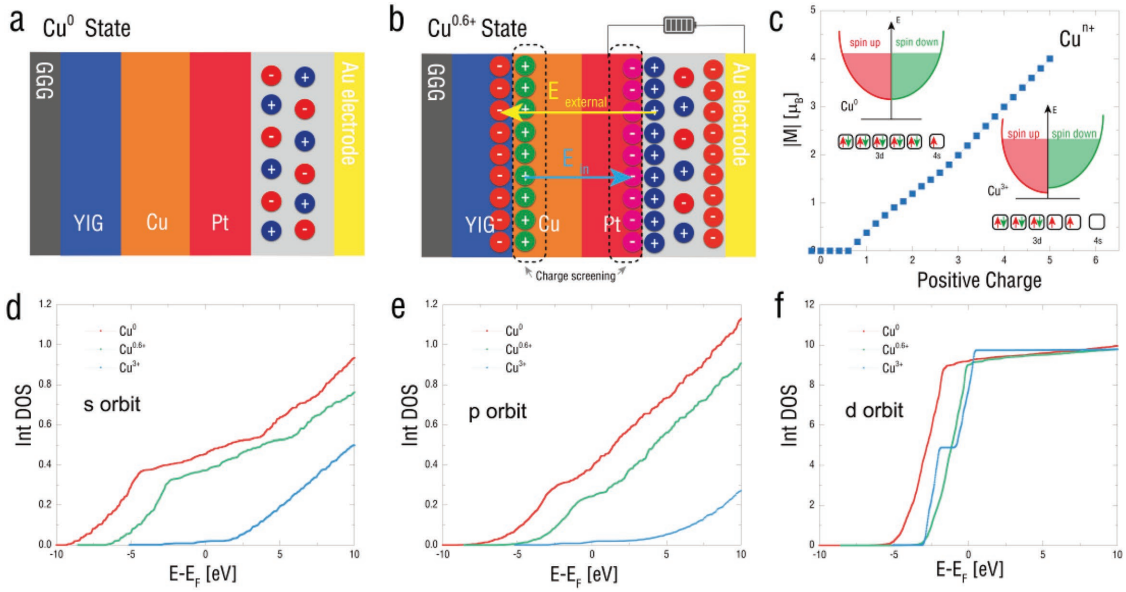

Figure 4. First-principle calculation of the induced magnetic moment of Cu with positive charge. a,b) The schematic of the Cu layer transform during the gating process. c) The magnetization as a function of positive charge. b–d) The integration of the DOS of Cu^0, $Cu^{0.6+}$, and Cu^{3+} for s, p, and d orbits, respectively.

(Supporting Information). These results illustrated that the H_r could be switched back and forth by applying negative and positive voltage across the IL layer at room temperature, indicating a good reversibility.

The MPE between YIG and heavy metals like Pt and Ta has been proved in many works, our result in Figure 1c also proves the existence of MPE in the interface of YIG and Pt. However, it has also been proved that there is almost no MPE between the YIG and light metal like Cu.[13,32,33] Recently, Ando and co-workers[15] found that the spin–torque generation efficiency of a $Cu/Ni_{81}Fe_{19}$ bilayer is enhanced by over two orders of magnitude by tuning the surface oxidation of Cu, reaching the efficiency of Pt/ferromagnetic metal bilayers. To a certain degree, the loss of electrons in the Cu atoms, which then form CuO_x, induces the magnetic change in the Cu layer. In our work, as YIG is an ideal insulator, the ILG voltage will induce an electron density change which is big enough to modulate the magnetic properties of Cu. Thus, the magnetic properties of the YIG/Cu/Pt heterostructure will change accordingly.

The first-principle calculations have been carried out to reveal the inner mechanism. Technically, we use the VASP code[34,35] to do all the calculations based on the density functional theory (DFT) and the generalized gradient approximation (GGA) with an interpolation formula according to Vosko, Wilk, and Nusair[36] and a plane-wave basis set within the framework of the projector augmented wave (PAW) method.[37,38] The cutoff energy for the basis was 500 eV, and the convergence criterion for the electron density self-consistency cycles was 10^{-6} eV. In the Brillouin zone, we sampled (15 × 15 × 15) k-point grids using the Monkhorst–Pack scheme[39] to make sure the results were converged.

In principle, the application of IL gating will generate a strong interfacial E-field on the sample. However, it is difficult to build up a chemical potential shift on metals due to the strong screening effect. The electrons of Cu layer will be forced to separate to the edge of the film by the sign of the charge, which is dependent on the direction of E-field. The electron accumulation on both sides of Cu/Pt can build up an opposite electric field to balance the external electric field (screening effect). When a positive gating voltage is applied in our case, we obtain a negative charge accumulation on Pt/IL interface and a positive charge accumulation on YIG/Cu interface theoretically distributed in the area less than 1 nm from the surface, which is also the origin of the electron depletion at YIG/Cu interface. These charge accumulations, however, also build a backward E-field to balance the E-field from IL. In this case, numerically, the charge number of Cu on at the Cu/IL interface will be the same as the applied voltage V_g, that is, Cun^-, $n = V_g$. On the contrary, the Cu on the interface between Cu and YIG will be Cun^+ to neutralize the total system. We start with Cun^+ first by removing electrons and then calculated the corresponding magnetization of Cu. As plotted in **Figure 4**c with increasing the positive charge of Cu, the nonmagnetic feature remains only about $Cu^{0.6+}$ and then comes up a magnetic state. This process is quite predictable as that the orbit of Cu is $3d^{10}4s^1$, so we need to take the $4s^1$ first and then the Hund rules can bring us the magnetization as that the unfilled d bands is the key issue for the magnetization in 3d materials. In this sense, the tendency of the magnetization of Cu as a function of the positive charge in Figure 4c can be understood directly. Moreover, for a clear view, the integration of density of states (DOS) of Cu^0, $Cu^{0.6+}$, and Cu^{3+} is analyzed in Figure 4d–f for s, p, and d orbit, respectively, where the integration to the Fermi energy stands for the occupation numbers. It can be seen that, below positive charge equals 0.6, only the occupation numbers of s and d orbit become smaller while that of d orbit is almost a constant. And when the positive charge is larger than 0.6 (Cu^{3+}),

the occupation numbers of d orbit decrease a lot while that of s and p orbits almost vanish, which confirms our previous analysis. To further clarify the principle in the gating experiment, we also characterized the surface charge accumulation as a function of the DC gating voltage (QV) in dry N_2 atmosphere as demonstrated in Figure S2a (Supporting Information) in green-round line. The surface charge density of the sample in N2 increased with the sequentially increasing gating voltage, and tend to saturate at 3 V, consisted with the Hr trend. The gating process had also been recorded in high vacuum environment, as shown in Figure S7. The results were similar to that in the N2 environment. These results are consistent with our previous observations, we believe that it is the electrostatic effect that dominated in the MPE gating manipulation process.

In this work, we achieved ionic modulation of the magnetic ordering in YIG/Cu/Pt heterostructure. We develop a YIG/Cu/Pt/IL/Au capacitor structure, the interfacial charge accumulation produces an FM ordering in the Cu near the Cu/YIG interface, thus an MPE-like coupling appeared in the YIG/Cu interface and influence the magnetic properties of the total system. Giant ME tunability up to 311 Oe V^{-1} is achieved via small gating voltage (<5 V) in the YIG/Cu/Pt heterostructure. The first-principle calculation reveals an E-field-induced FM ordering in Cu layer and corresponding FMR field tunability via the gating process. This novel IL gating of YIG/heavy metal system is of great research interest and practical significance for high-performance voltage-tunable YIG-based spintronic devices.

2. Experimental Section

Sample Preparation and Structural Properties: The YIG thin films were deposited onto (111)-oriented GGG substrates by pulsed laser deposition. The GGG (111) substrates were first ultrasonically cleaned with acetone, alcohol, and deionized (DI) water, subsequently. Then the substrate was mounted in the PLD chamber with the base pressure of 8.5×10^{-5} Pa, a commercial $Y_3Fe_5O_{12}$ ceramic was used as the target and a KrF excimer laser (Bruker D8 ADVANCE) was employed as the ablation source with 248 nm wavelength, 1 Hz repetition rate, and 240 mJ $pulse^{-1}$ laser beam energy. The substrate temperature was maintained at 800 °C, while the target–substrate distance was fixed at 60 mm. The YIG/GGG samples were then transferred to the off-axis magnetron sputtering chamber. Cu layer and Pt layer were deposited on the YIG samples, subsequently. The deposit power was set at 20 W to maintain a low deposit rate.

Magnetic Properties Measurements: The in-plane magnetic hysteresis loops of the samples were measured using a LakeShore 7404 vibrating sample magnetometer (VSM). FMR curves of the samples were measured using an X-band electron spin resonance (FMR) system (JOEL, JES-FA200). During the FMR test, the samples were located in the microwave cavity, the direction of the magnetic field was changed by rotating the sample. The test temperature can be changed using a temperature control kit.

The IL $[DEME]^+[TFSI]^-$ was chosen as the gating material for its potential tunability and well-studied physicochemical properties. A grid structure, Au/IL/Pt, was formed using Au and Pt as the gating electrode. Gating voltages from 0 to 4.8 V were performed to the grid structure using a Keysight B2901A Precision source/Measure Unit. In the IL phase, the anions and cations migrate toward the Au electrode and Pt electrode, respectively, driven by the E-field. The charge carrier particles generate an enormous surface charge density up to 10^{15} cm^{-2}, producing a strong interfacial E-field. The E-field influences on the magnetic properties of these samples were recorded by in situ FMR and VSM test. During the gating process, low-temperature FMR curves were performed in a cryogenic chamber by using liquid N_2.

Supporting Information

Supporting Information is available from the Wiley Online Library or from the author.

Acknowledgements

M.G., L.W., and S.Z. contributed equally to this work. The work was supported by the National Key R&D Program of China (Grant No. 2018YFB0407601), the Natural Science Foundation of China (Grant Nos. 51472199, 11534015, 51602244, and 51802248, 11804266), the Key R&D Program of Shaanxi Province (Grant No. 2018GY-109), the National 111 Project of China (B14040), China Postdoctoral Science Foundation (Grant Nos. 2016M590939 and 2018T111049), the Natural Science Foundation of Shaanxi Province (Grant No. 2017JQ5038) and the Shaanxi Province Science and Technology Innovation Project (Grant No. 2015ZS-02). The authors appreciate the support from the International Joint Laboratory for Micro/Nano Manufacturing and Measurement Technologies. The work at SFU was support by the Natural Science and Engineering Research Council of Canada (NSERC). We thank Dr. Chang Huang at Instrument Analysis Center of Xi'an Jiaotong University for their assistance with XRD analysis.

Conflict of Interest

The authors declare no conflict of interest.

Keywords

Cu magnetization, ferromagnetic resonance, ionic liquid gating, magnetoelectric coupling, yttrium iron garnet

Received: August 12, 2018
Revised: October 18, 2018
Published online: November 14, 2018

[1] K. Uchida, H. Adachi, T. An, T. Ota, M. Toda, B. Hillebrands, S. Maekawa, E. Saitoh, *Nat. Mater.* **2011**, *10*, 737.
[2] H. Nakayama, M. Althammer, Y. T. Chen, K. Uchida, Y. Kajiwara, D. Kikuchi, T. Ohtani, S. Geprags, M. Opel, S. Takahashi, R. Gross, G. E. Bauer, S. T. Goennenwein, E. Saitoh, *Phys. Rev. Lett.* **2013**, *110*, 206601.
[3] K. Uchida, S. Takahashi, K. Harii, J. Ieda, W. Koshibae, K. Ando, S. Maekawa, E. Saitoh, *Nature* **2008**, *455*, 778.
[4] D. Qu, S. Y. Huang, J. Hu, R. Wu, C. L. Chien, *Phys. Rev. Lett.* **2013**, *110*, 6.
[5] S. Y. Huang, X. Fan, D. Qu, Y. P. Chen, W. G. Wang, J. Wu, T. Y. Chen, J. Q. Xiao, C. L. Chien, *Phys. Rev. Lett.* **2012**, *109*, 107204.
[6] J. Sinova, *Nat. Mater.* **2010**, *9*, 880.
[7] H. Kurebayashi, O. Dzyapko, V. E. Demidov, D. Fang, A. J. Ferguson, S. O. Demokritov, *Nat. Mater.* **2011**, *10*, 660.
[8] Y. M. Lu, Y. Choi, C. M. Ortega, X. M. Cheng, J. W. Cai, S. Y. Huang, L. Sun, C. L. Chien, *Phys. Rev. Lett.* **2013**, *110*, 147207.
[9] C. Du, H. Wang, F. Yang, P. C. Hammel, *Phys. Rev. B* **2014**, *90*, 526.
[10] J. E. Losby, S. F. Fani, D. T. Grandmont, Z. Diao, M. Belov, J. A. Burgess, S. R. Compton, W. K. Hiebert, D. Vick, K. Mohammad, *Science* **2015**, *350*, 798.

[11] Y. Sun, H. Chang, M. Kabatek, Y. Y. Song, Z. Wang, M. Jantz, W. Schneider, M. Wu, E. Montoya, B. Kardasz, B. Heinrich, S. G. te Velthuis, H. Schultheiss, A. Hoffmann, *Phys. Rev. Lett.* **2013**, *111*, 106601.
[12] X. Z. Chen, R. Zarzuela, J. Zhang, C. Song, X. F. Zhou, H. A. Zhou, W. J. Jiang, F. Pan, *Phys. Rev. Lett.* **2018**, *120*, 207204.
[13] S. Emori, A. Matyushov, H. M. Jeon, C. J. Babroski, T. Nan, A. M. Belkessam, J. G. Jones, M. E. Mcconney, G. J. Brown, B. M. Howe, *Appl. Phys. Lett.* **2018**, *112*, 182406.
[14] V. Castel, N. Vlietstra, J. B. Youssef, B. J. V. Wees, *Phys. Rev. B* **2013**, *90*, 207.
[15] H. An, Y. Kageyama, Y. Kanno, N. Enishi, K. Ando, *Nat. Commun.* **2016**, *7*, 13069.
[16] Q. Yang, L. Wang, Z. Zhou, S. Zhao, G. Dong, Y. Chen, T. Min, M. Liu, *Nat. Commun.* **2018**, *9*, 991.
[17] S. Zhao, L. Wang, Z. Zhou, C. Li, G. Dong, L. Zhang, B. Peng, T. Min, Z. Hu, J. Ma, W. Ren, Z.-G. Ye, W. Chen, P. Yu, C.-W. Nan, M. Liu, *Adv. Mater.* **2018**, *30*, 1801639.
[18] Q. Yang, Z. Zhou, L. Wang, H. Zhang, Y. Cheng, Z. Hu, B. Peng, M. Liu, *Adv. Mater.* **2018**, *30*, 1800449.
[19] B. Cui, C. Song, G. A. Gehring, F. Li, G. Wang, C. Chen, J. Peng, H. Mao, F. Zeng, F. Pan, *Adv. Funct. Mater.* **2015**, *25*, 864.
[20] N. Lu, P. Zhang, Q. Zhang, R. Qiao, Q. He, H. B. Li, Y. Wang, J. Guo, D. Zhang, Z. Duan, Z. Li, M. Wang, S. Yang, M. Yan, E. Arenholz, S. Zhou, W. Yang, L. Gu, C. W. Nan, J. Wu, Y. Tokura, P. Yu, *Nature* **2017**, *546*, 124.
[21] S. Zhao, Z. Zhou, B. Peng, M. Zhu, M. Feng, Q. Yang, Y. Yan, W. Ren, Z. G. Ye, M. Liu, *Adv. Mater.* **2017**, *29*, 1606478.
[22] R. L. Fjerstad, *IEEE Trans. Microwave Theory Tech.* **1970**, *18*, 205.
[23] P. Roschmann, *IEEE Trans. Microwave Theory Tech.* **1973**, *21*, 52.
[24] G. Qiu, S. T. Chen, B. S. T. Wang, Y. Zhu, *IEEE Trans. Magn.* **2008**, *44*, 3123.
[25] A. S. Tatarenko, G. Srinivasan, M. I. Bichurin, *Appl. Phys. Lett.* **2006**, *88*, 183507.
[26] S. Ghosh, S. Keyvavinia, W. Van Roy, T. Mizumoto, G. Roelkens, R. Baets, *Opt. Express* **2012**, *20*, 1839.
[27] C. Kittel, J. F. Masi, *Phys. Today* **1957**, *10*, 43.
[28] J. J. Rhyne, R. W. Erwin, *Handb. Magn. Mater.* **1994**, *20*, 14/1.
[29] S. Y. Huang, X. Fan, D. Qu, Y. P. Chen, W. G. Wang, J. Wu, T. Y. Chen, J. Q. Xiao, C. L. Chien, *Phys. Rev. Lett.* **2012**, *109*, 1.
[30] H. Yan, Z. T. Zhang, S. H. Wang, H. R. Zhang, C. L. Chen, K. X. Jin, *ACS Appl. Mater. Interfaces* **2017**, *9*, 39011.
[31] B. Peng, Z. Zhou, T. Nan, G. Dong, M. Feng, Q. Yang, X. Wang, S. Zhao, D. Xian, Z. D. Jiang, *ACS Nano* **2017**, *11*, 4337.
[32] C. Hahn, G. D. Loubens, O. Klein, M. Viret, V. V. Naletov, J. B. Youssef, *Phys. Rev. B* **2013**, *87*, 2624.
[33] S. T. B. Goennenwein, R. Schlitz, M. Pernpeintner, K. Ganzhorn, M. Althammer, R. Gross, H. Huebl, *Appl. Phys. Lett.* **2015**, *91*, 140402.
[34] G. Kresse, J. Hafner, *Phys. Rev. B* **1993**, *48*, 13115.
[35] G. Kresse, J. Furthmüller, *Phys. Rev. B* **1996**, *54*, 11169.
[36] S. H. Vosko, L. Wilk, M. Nusair, *Can. J. Phys.* **1980**, *58*, 1200.
[37] B. Pe, *Phys. Rev. B* **1994**, *50*, 17953.
[38] G. Kresse, D. Joubert, *Phys. Rev. B* **1999**, *59*, 1758.
[39] H. J. Monkhorst, *Phys. Rev. B* **1976**, *16*, 1748.